19th Brazilian Congress of Thermal Sciences and Engineering
November 6th–10th, 2022, Bento Gonçalves - RS - Brazil

ENC-2022-0560
DISSOLVED OXYGEN HYDRODYNAMIC SIMULATION USING COUPLING WIND-BOTTOM SHALLOW WATER AND CONTAMINANT TRANSPORT FORMULATION IN ASUNCION BAY

Marcos G. Caceres [1]
Aida Ortiz [2]
School of Chemistry, National University of Asuncion, Paraguay
[1] mgcaceres@qui.una.py, [2] aidaortiz1995@gmail.com

Christian E. Schaerer
Polytechnic School, National University of Asuncion, Paraguay
cschaerer@pol.una.py

Diego H. Stalder
School of Engineering, National University of Asuncion, Paraguay
dstalder@ing.una.py

Laura Oporto
Dept. of Mathematical Sciences, University of Bath, UK
lcol20@bath.ac.uk

Abstract.
The Asuncion Bay is a naturally occurring water body with industrial and historical significance. Due to its geographical characteristics, it is a stopover for migratory birds. It is a protected wilderness area under the ecological reserve category, part of the Western Hemisphere Shorebird Reserve Network. Unfortunately, the bay is contaminated due to the lack of effective norms to process waste disposal. This work proposes a computational simulator to predict a reactive substance's hydrodynamics, Dissolved Oxygen (DO) concentration, and Biochemical Oxygen Demand (BOD). First, the mesh of the bay is obtained. Then, the hydrodynamics is solved through the Shallow Water Equations (SWE) modified with the shear stress of the bottom and the wind; at the same time, the transport equation is solved that includes the reactive terms of OD and BOD. The numerical simulation was performed in OpenFOAM, based on the finite volume method. The solver is verified numerically. Simulation results capture the dynamics qualitatively, predict the contaminant distribution in space and time in terms of DO, and identify critical stagnation regions in the bay. This is valuable information for decision-makers to avoid eutrophication and elaborate, precise mitigation actions for the natural conservation of Asuncion Bay.

Keywords: *Shallow Water Equations (SWE), Hydrodinamic Modeling, Dissolved Oxygen (DO), OpenFOAM, Asuncion Bay*

1. INTRODUCTION

Modern simulation tools (CFD) use numerical methods and algorithms to solve fluid transport problems for understanding the behavior of water bodies (Fringer *et al.*, 2006; Hongyang *et al.*, 2017). Numerical models can generate new knowledge about the behavior of water resources with little information and relatively low cost, as well as simulate different scenarios. This way, possible impacts can be predicted and valuable information generated when proposing solutions to several projects.

In Paraguay, Oporto *et al.* (2016) studied the influence of wind on the transport of a pollutant, considering the pollutant as a non-reactive passive scalar under the action of an external force (the wind) on Ypacarai Lake. They observed that changes in the wind direction alter the distribution of the pollutants across the lake, thus making it possible to identify

areas of more significant pollution for the different cases considered. Later, Bareiro *et al.* (2021) complemented the previous study, including bottom shear stress as an additional external force. As a result of these studies, it was possible to predict areas vulnerable to pollution.

This work proposes a simplified mathematical model for resolving the Navier Stokes equations for shallow waters. In the water model, the wind tensor and the bottom tensor are included since both are driving forces that define the movement of the pollutant in a body of surface water (Wu *et al.*, 2010). In addition, it is coupled to solve the transport equation of a scalar considering the reactive terms of DO and BOD because they are two critical indicators of water quality. The Dissolved Oxygen (DO), measured in mgO_2L, quantifies the concentration of oxygen present in the water. The Biochemical Oxygen Demand (BOD), also expressed in mgO_2L, represents a general measure of the concentration of Organic Matter (OM). The DO and OM parameters are related because organic matter needs oxygen to degrade (Orozco Barrenetxea *et al.*, 2003).

This article considers the Bay of Asuncion, which is a water system of high value for tourism development, trade, and environmental conservation. The last decade had important perimeter urban modifications related to filling works; urbanizations, road works (BID, 2004). Its main borders are 3 (three): to the southeast is the Coastal Strip, and within it is the beach of La Costanera; to the north, it is delimited by the San Miguel Bank, a stop for migratory birds, and the Nautical Club; and to the west is the strait that flows into the Paraguay River. The narrow opening limiting the Paraguay River gives the bay a geometry similar to that of a lake because the water located in the natural reservoir (average depth of 7.17m and surface area of $2.67km^2$) is only renewed by that border, increasing the possibility of stagnation areas. To understand the water flow behavior, it is necessary to analyze the hydrodynamics and the distribution of the pollutant, whose permanence in a specific region degrades the water quality. This highlights the need to investigate pollution risk zones based on computational simulations.

This paper is organized as follows: §2. presents the mathematical model, §3. describes the study area, parameters, mesh generation and the solver settings. Section 4. presents the simulation results. Finally §5. draws the conclusions.

2. MODEL DESCRIPTION

2.1 Hydrodynamics

Shallow Water Equations (SWE) are used to determine the velocity field. It is obtained by integrating the Navier-Stokes equations over depth.

First, we introduce two conservation principles, the conservation laws of mass and momentum. The continuity equation is a product of the law of conservation of mass, and it is expressed as Eq. (1),

$$\frac{\partial \mathbf{u_i} h}{\partial x_j} + \frac{\partial h}{\partial t} = 0. \tag{1}$$

In tensor form, the momentum equation is expressed as Eq. 2,

$$\frac{\partial \mathbf{u_i}}{\partial t} + \mathbf{u_j}\frac{\partial \mathbf{u_i}}{\partial x_j} = -g\frac{\partial}{\partial x_i}(h + z_0) + \frac{1}{h\rho}\frac{\partial}{\partial x_j}(h\tau_{ij}) - \frac{1}{h}\frac{\tau_{so,i}}{\rho} + \frac{1}{h}\frac{\tau_{wind,i}}{\rho}, \tag{2}$$

where x_j (j=1,2) represents the x and y axes, $\mathbf{u_i}$ (i = 1, 2) is the depth-averaged flow velocity ($u_1 = u$, $u_2 = v$) at x and y axes, h is the depth of the fluid, t is time, z_0 is the bottom elevation, τ is a tensor, τ_{so} and τ_{wind} are bottom shear stress and wind shear stress respectively, ρ is the density of water and g is the acceleration due to gravity.

Wu (1980) and Eid (1981) determined that the wind shear stress tensor is related to the wind speed by the following formula,

$$\tau_{wind,i} = \rho_{air} \cdot C_d \cdot \mathbf{U_{wind,i}} \left\|\mathbf{U_{wind}}\right\|, \tag{3}$$

where ρ_{air} is the air density, C_d is the drag coefficient, and $\mathbf{U_{wind}}$ is the wind speed at a given height, usually 10m.

Furthermore, Eid (1981) proposed that C_d can be obtained from wind speed and fetch which is a hydrodynamic concept that refers to the effective length of wind blow.

On the other hand, Tan (1992) defines the bottom shear stress by the following equation,

$$\tau_{so,i} = c_f \cdot \rho \cdot \mathbf{u_i} \left\|\mathbf{u}\right\|, \tag{4}$$

$$c_f = \frac{g \cdot n^2}{h^{1/3}}, \tag{5}$$

where c_f is the friction coefficient and n is defined as Manning's coefficient.

Manning's n coefficient depends only on the bottom characteristics, such as roughness or irregularities. This coefficient is highly studied since the values are obtained experimentally for both real and laboratory cases. The experimental data was collected and summarised in a table according to the characteristics of the body under study to help choose the appropriate coefficient (Farreras, 2006).

2.2 Water Quality

The concentration distribution of a chemical in water can be affected by convection, dispersion, diffusion, reaction, and sinks, or sources.

In lentic water environments such as lakes, bays, and reservoirs, diffusion tends to predominate. In these cases, the wind is the main agent that causes the mixture of water pollutants (Orozco Barrenetxea *et al.*, 2003).

Pollutant transport is represented by the second-order partial differential equation,

$$\frac{\partial c}{\partial t} + \mathbf{u_i} \cdot \nabla c = D\nabla^2 c + f_c, \tag{6}$$

where *c(x,y,z)* is the pollutant concentration and *D* is the diffusion coefficient. The term f_c represents all the additional interactions that may exist between them, such as chemical reactions, generation, or loss of the pollutant.

Furthermore, oxygen is a gas of low solubility in water necessary for aerobic aquatic life (Romero Rojas, 1999). Therefore, the most informative parameter to assess the contamination of a body of water is the BOD (Gomez, 2019), as it is a global measure of organic matter in mgL^{-1} (Orozco Barrenetxea *et al.*, 2003) and it is related to the amount of oxygen present in the body of study.

Considering that the system is free of flora, the reactive term f_c for the DO can be represented by Eq. (7). Here, the first term represents oxygen reaeration, the second one is related to oxidation and the last term is the oxygen demand by sediments (González-López and Ramírez-León, 2011),

$$f_{C_{DO}} = \frac{dC_{DO}}{dt} = k_r\theta_r^{(T-20)}(C_S - C_{DO}) - \ k_d\theta_d^{(T-20)}\left(\frac{C_{DO}}{k_{BOD}+C_{DO}}\right)C_{BOD} - \frac{S_{DO}}{h}\theta_s^{(T-20)}, \tag{7}$$

where C_{DO} is the concentration of dissolved oxygen, C_{BOD} is the biochemical oxygen demand concentration, C_S is the oxygen saturation concentration, k_r is the reaeration constant, k_d is the deoxygenation constant, k_{BOD} mean oxygen saturation constant, S_{OD} represents the oxygen demand of the sediments, $\theta_i^{(T-20)}$ is the Arrhenius expression for the rate constant adjustment for each constant, h is the depth and T is the temperature.

Regarding BOD in Eq. (8), the first term corresponds to oxidation and the second represents deposition,

$$f_{C_{BOD}} = \frac{dC_{BOD}}{dt} = -\ k_d\theta_d^{(T-20)}\left(\frac{C_{OD}}{k_{BOD}+C_{OD}}\right)C_{BOD} - V_S(1-f_{DS})C_{BOD}, \tag{8}$$

where V_S is the sedimentation velocity, and f_{DS} is the dissolved fraction of BOD.

2.3 Boundary Conditions

The bay boundary $\partial\Omega$ is divided into $\partial\Omega = \partial\Omega_S \cup \partial\Omega_D \cup \partial\Omega_R$, where $\partial\Omega_S$ corresponds to the boundaries where pollutants enter, $\partial\Omega_R$ represents the river boundary, and $\partial\Omega_D$ is the remainder of the bay boundary. For this last contour $\partial\Omega_D$, non-slip conditions are considered,

$$\mathbf{u} = \mathbf{u_{walls}} = 0 \longrightarrow \forall(x,y) \in \partial\Omega_D. \tag{9}$$

For pollutant inputs, an input flow condition is considered,

$$\mathbf{u} = \mathbf{u_{inlet}} \longrightarrow \forall(x,y) \in \partial\Omega_S. \tag{10}$$

Finally, there is a free flow condition at the bay-river boundary since both inflow and outflow occur in this zone, and there are no friction losses at the border, hence

$$\frac{\partial \mathbf{u_i}(x,y)}{\partial x_j} = 0 \longrightarrow \forall(x,y) \in \partial\Omega_R. \tag{11}$$

3. MODEL APPLICATION

The proposed model deals with the resolution of the SWE expressed in Eq. (1) and Eq. (2), two tensors are added to this equation: the tensor exerted by the wind and the tensor exerted by the bottom. At the same time, the transport equations of DO and BOD considered two scalars are solved (Eq. (6)). In the transport equations, the reactive term of both scalars presented in Eq. (7) and Eq. (8) are included.

3.1 Study area

The Asuncion Bay (Fig. 1) is a relatively small geographical feature located in the north of Asuncion, the capital of Paraguay. It has an area of 2.67km^2 and its limits cover 12.8km. Its maximum and average depths are 14.77m and 7.17m, respectively. To the north, it is limited by the Banco San Miguel, to the southeast with the Coastal Strip, and within it is the beach of La Costanera. There are also the three-channel that end on the bay. In the west, the bay limits the strait that flows into the Paraguay River.

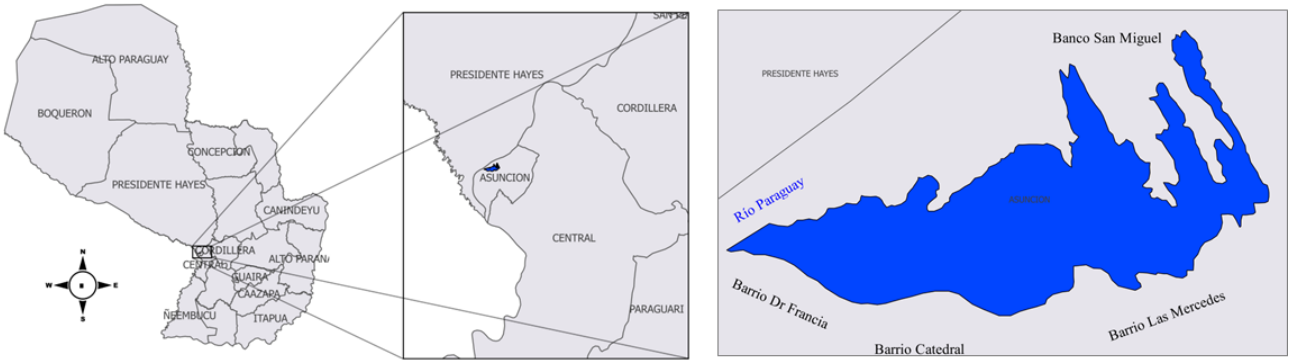

Figure 1. Location of the Asuncion Bay and its borders

Figure 2 shows the body with its corresponding inputs and outputs. The narrow border adjacent to the Paraguay River is considered mixed, the upper zone has an output condition, and the lower zone has an input condition, denoted as $F1_{in}$ and $F1_{out}$, respectively. The other entries correspond to the stream beds: Las Mercedes ($F2_{in}$) , Perú ($F3_{in}$) and Antequera ($F4_{in}$).

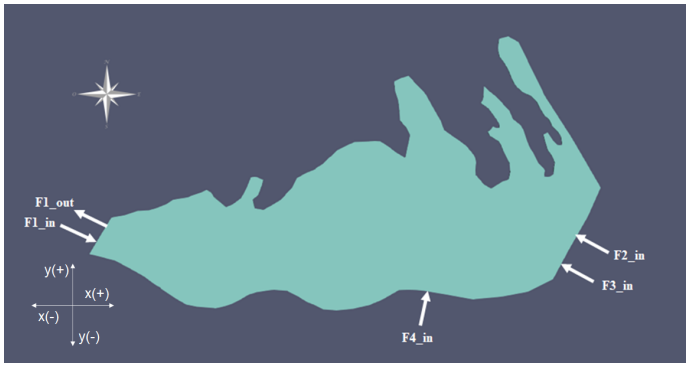

Figure 2. Boundary conditions

3.2 Parameters

Wind velocity data was provided by the Paraguayan Meteorology and Hydrology Directorate (DMH). These data are automatically collected by the anemometer located at the Costanera de Asuncion, which is part of the Paraguayan Network of Automatic Meteorological Stations. The data used was collected in two periods of time, corresponding to the months when field measurements were done. The predominant wind direction is west, with an average speed of 2.6 ms^{-1}.

Table 1 details the values of the parameters required by the SWE. Two values are assumed for the Manning Coefficient n according to the type of bottom surface that the bay has. In the Banco San Miguel areas, n is 0.045 due to the presence of small bushes and grasses, and in the rest of the surface, the constant takes a value of 0.03 considering that the bay is a natural course on the plain without major faults. To determine the drag coefficient C_d, a fetch of 1km and average wind speed of 4.79ms^{-1} (Báez, 2015) are considered, leaving the drag coefficient as $0.95 \cdot 10^{-3}$.

Table 2 details the values of the parameters extracted from the literature to replace them in Eq. (7) and Eq. (8) and be able to determine the distribution of OD and BOD.

The temperature assumed for the simulations is 25°C, it is considered to remain constant throughout the process, and those temperature-dependent parameters are corrected by the Arrhenius equation using the values shown in Tab. 2.

Table 1. Parameters used in the hydrodynamic simulation

Parameter	Symbol	Value
Water density (kgm^{-3})	ρ	1000
Dynamic viscosity of water ($kgm^{-1}s^{-1}$)	μ	8,937 $\cdot 10^{-4}$
Air density (kgm^{-3})	ρ_{air}	1.29
Wind speed (ms^{-1}) (1)	u_{air}	2.6
Wind drag coefficient (dimensionless) (2)	C_d	0.95 $\cdot 10^{-3}$
Manning's coefficient (dimensionless) (3)	n	0.03 and 0.045
Gravity (ms^{-2})	g	9.81

(1) DMH Data (2018)
(2) Eid (1981)
(3) Chow (1994)

Table 2. Parameter values in the OD and BOD Model

Parameter	Symbol	Value
Oxygen saturation concentration (mgO_2L^{-1}) (1)	C_s	8,176
Reaeration constant (day^{-1}) (2)	k_r	0,49
Deoxygenation constant (day^{-1}) (3)	k_d	0,037
Mean oxygen saturation constant (mgL^{-1})) (4)	k_{DBO}	0,5
Oxygen demand of the sediments ($gm^{-2}day^{-1}$) (2)	S_{OD}	0,288
Arrenihus constant (dimensionless) (5)	θ_r θ_d θ_s	1,028 1,047 1,08
Dissolved fraction (dimensionless) (4)	f_{DS}	0,5
Sedimentation velocity ($mday^{-1}$) (5)	V_S	0,1

(1) Elmore and Hayes (1960)
(2) Bowie *et al.* (1985)
(3) Cárdenas (2005)
(4) Piasecki (2002)
(5) Wool *et al.* (2006)

The boundary conditions for the concentrations of the species are taken considering the limit values defined in the resolution of the SEAM (2002) for Class 3 waters: waters destined for secondary contact recreation, of a maximum of BOD is $10mgO_2L^{-1}$, and DO not less than $4mgO_2L^{-1}$. As reported by Maidana (2020), the velocities of the outlets are as follows: Las Merecedes ($F2_{in}$) has a value of $0.0854ms^{-1}$, Peru ($F3_{in}$) equals $0.0708ms^{-1}$ and Antequera($F4_{in}$) equals $0.0523ms^{-1}$.

The initial BOD is assumed to have a value of $0mgO_2L^{-1}$ and the initial OD is equal to the oxygen saturation concentration. The simulation start time is 0s, the end time is 3000000s with a time step of Δt = 1s.

3.3 Mesh Generation and Independence Test

To carry out the numerical simulation, the mesh is first generated; the free software QGIS (QGIS Development Team, 2018) is used to process the bathymetric data and generate contour lines of the Bay, then these contour lines are exported to the free software Salome-Meca (Code_Aster, 2017) to generate the mesh. The type of mesh obtained is mixed with quadrangular geometry in the areas near the border and triangular geometry in the rest of the body, defined with Salome's *sub-mesh* tool. Once the mesh is obtained, it is necessary to verify that the simulation results are independent of the mesh refinement level.

Spatial convergence is achieved by performing the grid independence test. Simulations are run at different refinement levels, R_1 and R_2 (details in Tab. 3), to choose the refinement that adequately represents the behavior of the field of study using the lowest possible computational cost.

Independence is evaluated considering 3 final simulation times: 50000, 100000, and 200000 s. From the results of the simulations, values are taken on the trajectory of the maximum length of the bay and the data are processed for quantitative analysis, finding the Mean Absolute Percentage Error (MAPE), and the Mean Square Error (MSE); the results of the evaluations are seen in the Tab. 4.

Table 3. Generated and refined meshes

Mesh	Number of Total Elements	Average Cell
Unrefined (UR)	9312	79,45m^3
Refined 1 (R_1)	24712	29,95m^3
Refined 2 (R_2)	34706	21,32m^3

Table 4. Mesh Independence Test Evaluation

Simulation time	MAPE		MSE	
	UR-R_2	R_1-R_2	UR-R_2	R_1-R_2
50.000s	39 %	33 %	0,00444	0,00425
100.000s	42 %	44 %	0,00228	0,00199
200.000s	33 %	22 %	0,00326	0,00318

It is observed that the refinement mesh R_1 presented in Fig. 3 gives greater precision for UR, considering that the values obtained in R_2 are the real ones. In addition, R_1 has a lower computational cost than R_2; considering the time 200000s, the total real-time is equal to 24488s and 33898s for R_1 y R_2, respectively.

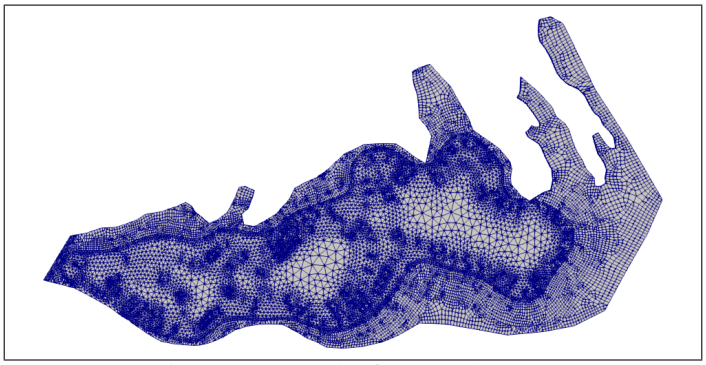

Figure 3. R_1 mesh of 24712 elements

3.4 Time independence test

Once the mesh is chosen, the time independence test is performed by evaluating different time steps to optimize the simulation speed and computational cost. For the analysis, 3-time steps of 0.5s are chosen; 1s and 1.5s. The final simulation time is defined as 100000s for the 3 cases.

The simulation with a 1.5s time step presents an error of convergence. This is due to the increase in the Courant CFL number (high time step), reaching a value of 2.046s at 8.436s of simulation. Hence, this time step is discarded. On the other hand, the velocity profiles for the 0.5s and 1s time steps are very similar, as seen in Fig. (4.a) and Fig. (4.b). Over the maximum length, the Root Mean Square Error is $1.42 \cdot 10^{-5}$, so the time step of 1s is chosen due to the advantage in processing time that is less.

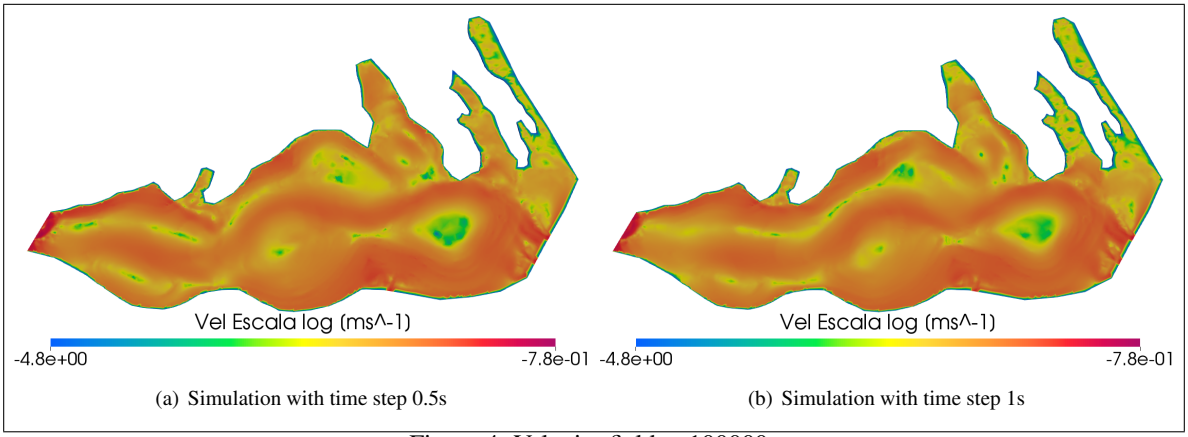

(a) Simulation with time step 0.5s (b) Simulation with time step 1s

Figure 4. Velocity field at 100000s

3.5 Description of solver and numerical verification

OpenFOAM has a directory with different solvers for incompressible streams (Greenshields, 2020). The solver used in this work is based on *shallowWaterFoam*, which is a solver for the SWE shown in Eq. (2). Our modified solver includes two scalar fields corresponding to OD and BOD to solve the transport equation for each one, and the corresponding reactive term is added to each transport equation (Eq. (7) and (8)). The scheme of the modified solver algorithm is shown in Fig. 5.

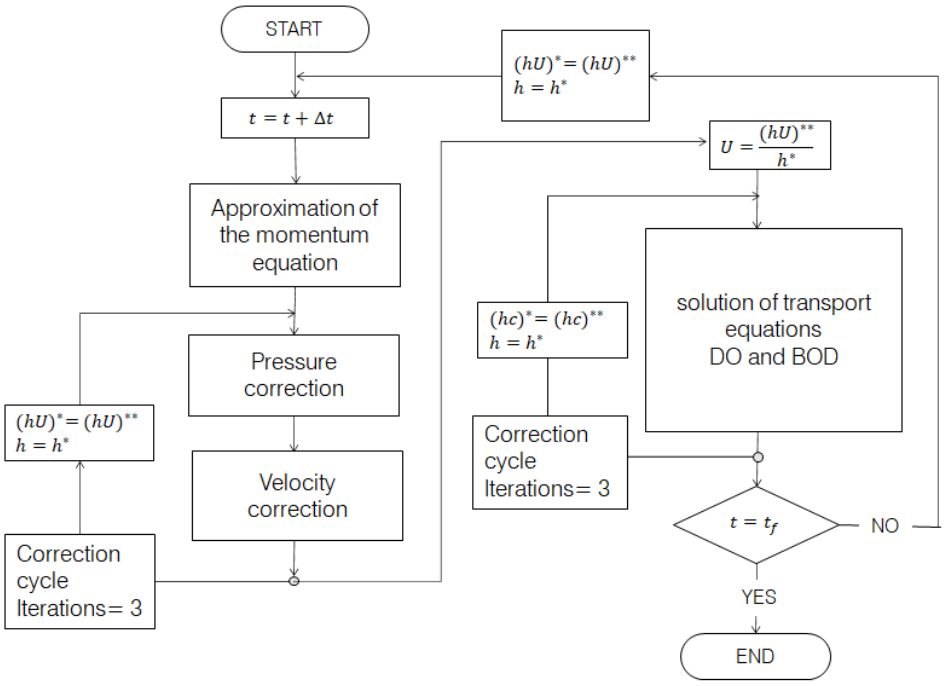

Figure 5. Scheme of the algorithm

We solve the system using the PIMPLE algorithm. It begins with a predictor step of the velocity, where the depth h is considered constant with respect to the previous time, as well as the value of hU in terms of convection, diffusion, and background stress. Thus, obtaining the new value $(hU)^*$. Corrections are made with the pressure term where a new h^* is found and used in the next step to correct the velocity and obtain the term $(hU)^{**}$. With the obtained values of $(hU)^{**}$ and h^*, we calculate U, which is introduced in the scalar transport equations to find OD and BOD, but since their equations are codependent, this is done in an iterative cycle. This whole process is repeated until the simulation time is complete.

For the validation of the solver, initially, code verification is performed; since the OpenFOAM base solver was modified, *shallowWaterFoam*. Results obtained from the solver are contrasted with analytical solutions to verify that equations are appropriately solved. Only the terms corresponding to Dissolved Oxygen and BOD are analyzed.

In this step, the comparison is performed on a unidimensional mesh using the analytical Streeter Phelps model (Streets and Phelps, 1925). The model includes Eq. (12) and Eq. (13):

$$u\frac{dC_{BOD}}{dx} = -k_d C_{BOD}, \tag{12}$$

$$u\frac{dD}{dx} = -k_d C_{BOD} + k_r D, \tag{13}$$

where u is the velocity of the fluid on the x direction; C_{BOD} is the BOD concentration in $\text{mgO}_2\text{L}^{-1}$; k_d the deoxygenation constant in s^{-1}; k_r is the reaeration constant in s^{-1} and D is the deficit of the Dissolved Oxygen concentration with respect to the Saturation concentration C_S: $D = C_S - C_{DO}$ in $\text{mgO}^2\text{L}^{-1}$. The analytical solutions of the Eq. (12) and Eq. (13) are written in Eq. (14) and Eq. (15):

$$C_{BOD} = C_{BOD_0} e^{-k_d x/u}, \tag{14}$$

$$D = \frac{k_d C_{BOD_0}}{k_r - k_d}\left(e^{-k_d x/u} - e^{k_r x/u}\right) + D_0 e^{-k_r x/u}, \tag{15}$$

where C_{BOD_0} and D_0 correspond to the initial values of BOD and Dissolved Oxygen deficit, respectively.

The comparison between numerical results obtained by the solver and the Streeter Phelps analytical solution is presented in Fig. 6.

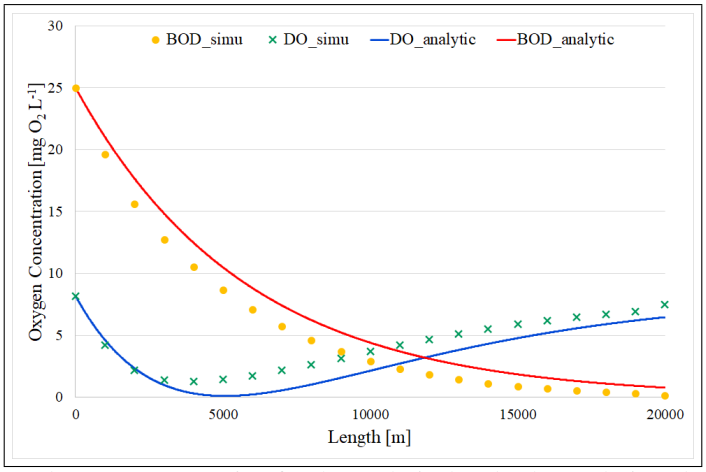

Figure 6. DO and BOD concentration for the analytical and solver solution along the x axis

Figure 6 shows that the numerical and analytical results are very similar. The minor differences are due to the terms not being considered in the Streeter Phelps model. Hence, we conclude that the solver captures the desired solution.

4. SIMULATION RESULTS

4.1 Hydrodynamic Simulation

Meshes of different sizes were generated. After performing a mesh and time independence test, the chosen mesh has 24712 elements, and a time step of 1s was taken for the simulation, performing it up to 3000000s. For the simulations, a laminar flow was considered throughout the domain due to the handled low velocities.

Figure 7 shows the velocity field in the analysis area. The velocities are represented on a logarithmic scale to appreciate the differences better. The areas with low speeds are those close to Banco San Miguel. In this region, there are sandbanks with small bushes, and the roughness considered in this sector is more significant than in the rest of the study area. There are also low velocities in the most profound areas, and the flow lines pass around them because the velocity gradients are produced by the differences in depth in the study body.

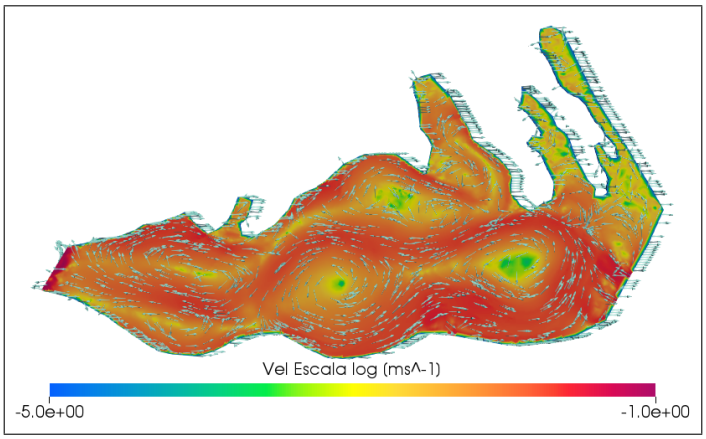

Figure 7. Velocity vector field in the study area

4.2 Distribution of DO and BOD

Figure 8 shows both the distribution of the DO concentration and BOD. The DO concentrations are low in the areas near the tributaries. However, the BOD has the highest concentrations in that area. The contaminant that enters the system initially with high BOD, acquires the hydric movement of the bay. In this path, the initially saturated oxygen in the

fluid degrades the OM, decreasing the BOD, so the distribution concentrations have fields similar to each other, and their behavior tends to the hydrodynamics of the fluid.

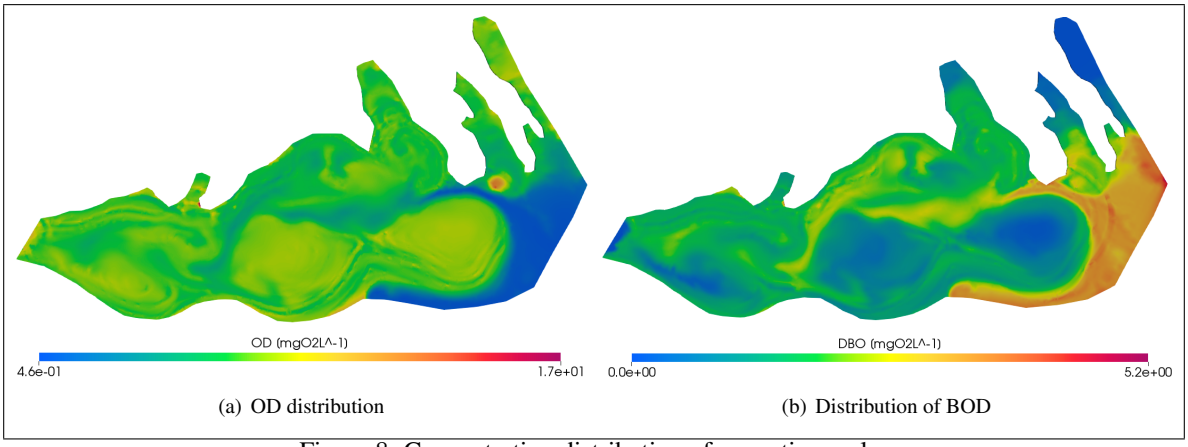

(a) OD distribution (b) Distribution of BOD

Figure 8. Concentration distribution of a reactive scalar

The maximum BOD concentration at 3000000s is 5.2 mgO_2L^{-1}, which decreases approximately 50% of the initial concentration. This is the maximum concentration observed in the area corresponding to the inlets of the tributaries, which coincides with the lowest values of oxygen concentrations. In this zone, the residence time is enough for the oxygen to degrade the BOD as much as possible. However, there is not enough oxygen to completely degrade the BOD or reach a low BOD level as a considerable amount of oxygen is invested in the degradation process. Because the oxygen level is the lowest in this system area, the BOD consumption rate also decreases. Therefore, one can see that the BOD concentration is higher in the entrance areas as there is a lower consumption rate per deoxygenation process. It is corroborated that the DO and BOD concentration fields have inverse behavior, i.e., the DO is low when the BOD is high and vice versa. There are low concentrations of DO near the entrance areas of the tributaries.

Considering that there are no previous similar computational studies on the Bay, and there was not enough measurement equipment to obtain a large number of measurements in the location, only qualitative analysis can be carried out. Even so, this qualitative approach provides results similar to the behavior of the Bay.

5. CONCLUSIONS

This article presents a water model that considers the effects of the wind and bottom tensor on the fluid's movement and a water quality model that shows the distribution of DO and BOD of a reactive substance discharged in a body of a shallow water model. OpenFOAM free software is used for resolution and post-processing.

Applying the hydric and water quality models proposed to Asuncion Bay, it is observed that the results are qualitatively corresponding in terms of the movement of the fluid and the distribution of the reactive contaminant. The hydrodynamics showed that the flow of water tends to have a movement corresponding to the bay's contour lines. The zones with the lowest speeds are identified in the arms of the bay, and the deepest ones, these zones are the ones that require special care because they are points of stagnation in the bay.

The distribution of DO and BOD have similar characteristics. It was observed that in the areas of Banco San Miguel, both the value of BOD and DO concentrations remained low. This is a consequence of the low velocities in the zone, which implies a longer residence time of the scalar and allows its degradation. In areas with higher speeds, this degradation cannot occur, so despite a high DO and BOD value, oxygen is not used by the organic matter to oxidize and pass into its simplest form.

The model allows analyzing the temporal and spatial evolution of the velocity, DO, and BOD concentrations, identifying the minimum and maximum values that are reached, thus determining the most critical areas from the point of view of water quality. Therefore, it can be applied to similar bodies of water. The results obtained in this article help to focalize a Management Plan of the Ecological Reserve of Asuncion Bay and the San Miguel Bank. It is also possible to analyze the behavior of the bay with different scenarios varying the parameters involved to help decision-makers execute of the Comprehensive Sanitation Plan for Asuncion Bay.

6. ACKNOWLEDGEMENTS

Authors acknowledge the Laboratorio de Computación Científica y Aplicada (LCCA) from Facultad Politécnica, the Dirección de Meteorología e Hidrología del Paraguay (DMH), and the Administración Nacional de Navegación y Puertos (ANNP).

7. REFERENCES

Báez, J., 2015. "Mapa de velocidad del viento". URL https://cta.uc.edu.py/mapa-de-velocidad-del-viento/. Online; accedido 01/08/20.

Bareiro, D., O'Durnin, E., Oporto, L. and Schaerer, C.E., 2021. "Shallow water model for pollutant distribution in the ypacarai lake". *Rev. Soc. cient. Parag*, pp. 54–76.

BID, 2004. "Programa de desarrollo de la franja costera de asunción bid (pr-0143)". Relatorio de impacto ambiental(rima), Banco Interamericano de Desarrollo, Municipalidad de Asunción, Abt Associates Inc, Paraguay. URL https://bahiaasuncion.files.wordpress.com/2008/05/iadbpublicdoc-rima-franja-costera.pdf.

Bowie, G.L., Mills, W.B., Porcella, D.B., Campbell, C.L., Pagenkopf, J.R., Rupp, G.L., Johnson, K.M., Chan, P., Gherini, S.A. and Chamberlin, C., 1985. "Rates, constants, and kinetics formulations in surface water quality modeling". *EPA*, Vol. 600, pp. 3–85.

Chow, V.T., 1994. *Hidraulica de Canales Abiertos*. McGRAW-HILL, Bogotá [Colombia].

Code_Aster, 2017. "Salome-platform". URL https://qgis.org/es/site/. Online; accedido 19/11/19.

Cárdenas, J., 2005. *Calidad de Aguas para estudiantes de Ciencias Ambientales*. Universidad Distrital Francisco Jose de Caldas.

Eid, B.M., 1981. *Investigation into interfacial transports and exchange flows for lake models*. Ph.D. thesis.

Elmore, H. and Hayes, T., 1960. "Solubility of atmospheric oxygen in water". Vol. 86, pp. 41–53.

Farreras, S., 2006. "Hidrodinámica de lagunas costeras". *Mexico: Centro de Investigación Científica y de Educación Superior de Ensenada*.

Fringer, O.B., Gerritsen, M. and Street, R.L., 2006. "An unstructured-grid, finite-volume, nonhydrostatic, parallel coastal ocean simulator". *Ocean modelling (Oxford)*, Vol. 14, No. 3, pp. 139–173. ISSN 1463-5003. doi: 10.1016/j.ocemod.2006.03.006.

Gomez, V., 2019. "Tipos de modelos que se aplican a estudio de la calidad del agua". URL https://www.lifeder.com/tipos-modelos-apliquen-estudio-calidad-agua/.Cop. Accedido 24/03/21.

González-López, R. and Ramírez-León, H., 2011. "Modelación numérica de la hidrodinámica, del oxígeno disuelto y la demanda bioquímica de oxígeno en sistemas con vegetación". *Hidrobiológica*, Vol. 21, No. 2, pp. 147–158. ISSN 0188-8897.

Greenshields, C.J., 2020. *OpenFOAM v8 User Guide*. URL http://foam.sourceforge.net/docs/Guides-a4/OpenFOAMUserGuide-A4.pdf. Online; accedido 01/10/20.

Hongyang, L., Jianyu, H., Jia, Z., Cheng, P., Chen, Z., Zhenyu, S. and Chen, D., 2017. "Tide- and wind-driven variability of water level in sansha bay, fujian, china". *Frontiers of earth science*, Vol. 11, No. 2, pp. 332–346. ISSN 2095-0195. doi:10.1007/s11707-016-0588-x.

Maidana, E., 2020. "Determinación cuantitativa de microplásticos en muestras de agua de los cauces hídricos que desembocan en la bahía de asunción".

Oporto, L.C., Ramírez, D.A., Varela, J.D. and Schaerer, C.E., 2016. "Analysis of contaminant transport under wind conditions on the surface of a shallow lake". *Mecánica Computacional*, Vol. 34, No. 31, pp. 2155–2163.

Orozco Barrenetxea, C., Pérez Serrano, A., Gonzalez Delgado, M.N., Rodríguez Vidal, F.J. and Alfayate Blanco, J.M., 2003. *Contaminacion ambiental: Una vision desde la quimica*. Paraninfo. ISBN 8497321782.

Piasecki, M., 2002. *Optimization of In-Stream Dissolved Oxygen Via Control of CBOD Loadings Using the Adjoint Method*, pp. 547–565.

QGIS Development Team, 2018. "Qgis 2.18". URL https://qgis.org/es/site/. Online; accedido 20/01/20.

Romero Rojas, J.A., 1999. *Tratamiento de aguas residuales, teoría y principios de diseño*. ISBN 978-958-8060-13-2.

SEAM, 2002. "Resolución 222: Padrón de calidad de las aguas en el territorio nacional".

Streets, H. and Phelps, E., 1925. "Study of the pollution and natural purification of the ohio river, iii, factors concerned in the phenomena of oxidation and reaeration, us public health service". *Public Health Bulletin*, Vol. 146.

Tan, W.Y., 1992. *Shallow water hydrodynamics: Mathematical theory and numerical solution for a two-dimensional system of shallow-water equations*. Elsevier. ISBN 0080870937.

Wool, T.A., Ambrose, R.B., Martin, J.L., Comer, E.A. and Tech, T., 2006. "Water quality analysis simulation program (wasp)". *User's Manual, Version*, Vol. 6.

Wu, J., 1980. "Wind-stress coefficients over sea surface near neutral conditions - a revisit". *Journal of physical oceanography*, Vol. 10, No. 5, pp. 727–740. doi:10.1175/1520-0485(1980)010<0727:WSCOSS>2.0.CO 2.

Wu, X., Kong, F., Chen, Y., Qian, X., Zhang, L., Yu, Y., Zhang, M. and Xing, P., 2010. "Horizontal distribution and transport processes of bloom-forming microcystis in a large shallow lake (taihu, china)". *Limnologica*, Vol. 40, No. 1, pp. 8–15.

8. RESPONSIBILITY NOTICE

The authors are solely responsible for the printed material included in this paper.